MANSOURA JOURNAL OF CHEMISTRY
Official Journal of Faculty of Science, Mansoura University, Egypt
E-mail: scimag@mans.edu.eg ISSN: 2974-4938

Enhanced Electrochemical Performance of $Er_2O_3/ZnWO_4$ Composite for High-Efficiency Supercapacitor Applications.

Menna A. Khder[a,b], *E. A. El-Sharkawy*[c], *Awad I. Ahmed*[a,b]

[a] Department of Chemistry, Faculty of Science, Mansoura University, Al-Mansoura 35516, Egypt.

[b] Energy & Desalination Center, Faculty of Science, Mansoura University, Egypt

[c] Department of Chemistry, Faculty of Science, Suez University, Suez, Egypt.

*** Correspondence to:** mennaakhderr@gmail.com, 01555703336

Received:25/5/2025
Accepted:28/5/2025

Abstract: This study investigates the electrochemical performance of $ZnWO_4$ and $Er_2O_3/ZnWO_4$ composites as potential supercapacitor electrode materials. Using cyclic voltammetry (CV), galvanostatic charge-discharge (GCD), and electrochemical impedance spectroscopy (EIS), the capacitive behavior, charge transfer kinetics, and stability of the materials were thoroughly evaluated. Results demonstrate that the $Er_2O_3/ZnWO_4$ composite exhibits significantly enhanced specific capacitance and longer discharge time compared to pure $ZnWO_4$ alone. This improvement is attributed to the increased pseudocapacitive contribution from Er_2O_3 and its synergistic interaction with $ZnWO_4$. Nyquist plot analysis revealed a lower charge-transfer resistance and better ion diffusion in the composite, indicating improved faradaic activity and efficient charge storage. The synergistic effect between Er_2O_3 and $ZnWO_4$ enhances both energy storage capability and cycling stability. These findings highlight the $Er_2O_3/ZnWO_4$ composite as a promising and efficient electrode material for high-performance supercapacitors, offering excellent and superior electrochemical characteristics over $ZnWO_4$ alone, and promising durability for future energy storage devices.

keywords: rare earth metal, energy, zinc tungstate, supercapacitor

1. Introduction

The rapid growth in energy demand and environmental issues has spurred substantial research into advanced energy storage devices [1-3]. Supercapacitors, or electrochemical capacitors, have emerged as a novel type of energy storage solution, drawing significant interest from researchers in fields such as electronics, devices, and electric vehicles. This interest is due to supercapacitors' high-power density, long cycle life, broad operating temperature range, safe performance, eco-friendliness, and affordability. Supercapacitors offer a power density higher than that of batteries and an energy density greater than that of traditional capacitors. Based on their energy storage mechanism, supercapacitors are classified into two categories: electrochemical double-layer capacitors (EDLCs) and pseudocapacitors. Generally, carbon-based materials (like activated carbon, carbon nanotubes, carbon aerogels, and graphene oxide) exhibit EDLC behavior, while materials with redox properties (such as metal oxides and conducting polymers) show pseudocapacitance. A key limitation of EDLCs is the structural breakdown of carbon-based materials during cycling, which affects their stability. In pseudocapacitors, the faradaic reactions occur both on the electrode surface and within its bulk, resulting in higher capacitance and enhanced cycle stability compared to EDLCs. However, selecting appropriate electrode materials is crucial for achieving high specific capacitance in pseudo capacitors [4-6]. Recently, tungstate-based binary metal oxides have attracted significant interest due to their favorable properties, such as eco-friendliness, making them well-suited for pseudocapacitor applications [7-8]. Zinc tungstate ($ZnWO_4$), part of the AWO_4 family, is a notable material

that can crystallize in either the scheelite or wolframite structure. $ZnWO_4$ is isostructural with $ZnWO_4$ and $CdWO_4$, featuring a monoclinic wolframite-type structure within the $P_{2/c}$ space group [9]. Beyond energy storage, $ZnWO_4$ is also widely used in fields like photocatalysis and gas sensing, thanks to its beneficial physical and chemical characteristics. Moreover, $ZnWO_4$ serves as an effective electrode material for supercapacitors, as both zinc and tungsten exhibit electrochemical activity [10-11]. Blending transition and inner transition metal oxides have garnered significant attention due to their potential applications in various scientific and technological fields. Their favorable capacitive properties and eco-friendliness make them promising candidates as electrode materials for supercapacitors [12].

Rare earth elements possess unique characteristics, including variable oxidation states, diverse coordination numbers, 4f-electron transitions with multiple conformational states, and vacant sites in crystal structures, distinguishing them from transition metals [13]. Furthermore, the great stability of these components in solutions has allowed the development of electrodes with exceptional reproducibility and endurance [14]. Erbium, in particular, is coveted for its use in optical communication technology, high-performance luminous devices, and as a component of different electrocatalysts. Erbium oxide (Er_2O_3) is a unique substance with potential applications as a catalyst in sensors, biosensors, supercapacitors, and photodegradation. Its effectiveness is due to its distinctive features, which include a high specific heat capacity, semiconducting nature, and low toxicity [15-16]. Herein, combining Er_2O_3 and $ZnWO_4$ produced a composite material with improved performance, particularly for supercapacitors. Erbium doping altered the electronic structure of $ZnWO_4$, potentially enhancing conductivity and introducing new active sites for charge storage. This hybrid technique takes advantage of the unique qualities of both materials to obtain high energy density, great stability, and a longer cycle life. Researchers are investigating such combinations to push supercapacitor performance beyond standard materials, making them appropriate for applications that require quick charge and discharge capabilities, such as electric vehicles and portable gadgets.

2. Experimental

2.1. Materials and chemicals

Every chemical used was sourced from a commercial source without any further purification. Zinc nitrate hexahydrate (98%), Erbium nitrate pentahydrate (99.9%), and Sodium tungstate dihydrate were obtained from Sigma Aldrich. Deionized water (DI) (18 M cm) was obtained from the Millipore water system used to prepare all aqueous solutions.

2.2. Synthesis of $Er_2O_3/ZnWO_4$

The $Er_2O_3/ZnWO_4$ composite was synthesized via the calcination co-precipitation method. Initially, stoichiometric amounts of Zn $(NO_3)_2 \cdot 6H_2O$ and Er $(NO_3)_3 \cdot 5H_2O$ in a 1:1 molar ratio were dissolved in deionized (DI) water under constant stirring for 30 minutes to ensure homogeneous mixing. Subsequently, a $Na_2WO_4 \cdot 2H_2O$ solution was carefully introduced dropwise into the mixture until a pink precipitate was observed. The precipitate was thoroughly washed with DI water to remove any residual ions. The collected precipitate was then dehydrated by heating at 80 °C for 6 hours. Finally, the dried powder underwent calcination at 500 °C in an air atmosphere for 2 h to obtain $Er_2O_3/ZnWO_4$. The $ZnWO_4$ sample was synthesized following the same procedure as described for $Er_2O_3/ZnWO_4$, with the only modification being the exclusion of Er $(NO_3)_3 \cdot 5H_2O$ from the initial reactant mixture.

2.3. Material Characterization

Various methods of analysis were employed to verify the effectiveness of the preparation. SEM (JEOL JSM 6510LV) was used to investigate the materials' crystalline phase. The crystal structure at the 2θ range of 5°–70 was characterized by X-ray diffraction (XRD) patterns performed with a Bruker equipment (λ = 1.54178 Å, step size of 0.02 and scan step length of 0.80 s). In addition, FT-IR patterns (FT-DATR in the wavenumber range of 500 to 4000 cm) observed with a MATTSON IR-5000S spectrophotometer, whose total reflectance was decreased by a diamond, were used to monitor the functional groups in the

structure. The catalysts were electrochemically analysed using Corrtest CS350, then the resulting data was fitted with CS workstation software.

2.5. Electrochemical Performances

A three-electrode cell setup was employed to conduct electrochemical measurements using 3.0 M KOH as the electrolyte at an ambient temperature. The synthesized materials, deposited on nickel foam (NF), acted as the working electrodes (WE), with platinum foil as the counter electrode (CE) and Hg/HgO as the reference electrode (RE). An electrochemical workstation facilitated the primary electrochemical analyses, including galvanostatic charge-discharge (GCD), cyclic voltammetry (CV), and electrochemical impedance spectroscopy (EIS).

To prepare the electrodes, an activation process was first carried out with 50 CV cycles at a scan rate of 50 mV/s. CV measurements were subsequently performed over a voltage window of 0 to 0.6 V at varying scan rates from 1 to 100 mV/s. GCD profiles were collected within the same voltage range, at current densities of 1, 5, 7, 10, and 20 A g^{-1}. EIS data were acquired across a frequency spectrum from 10^5 Hz to 10^{-2} Hz at an open-circuit potential (OCP) with a 5-mV amplitude.

3. Results and Discussion

3.1. Specifications of the Material

The composition and phase structure of the products were first analyzed by X-ray diffraction (XRD) as shown in Fig.1.

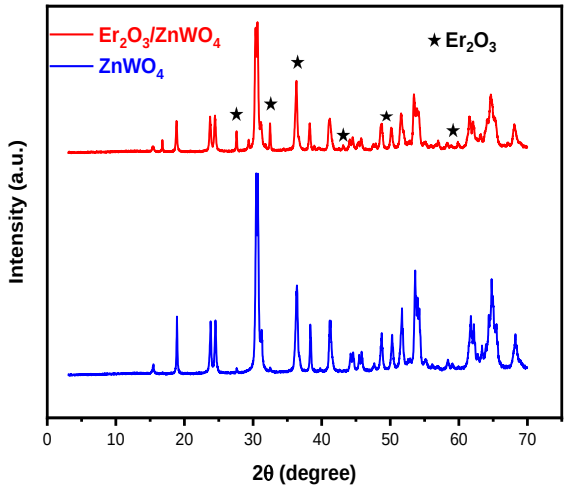

Fig.1. XRD patterns of Er_2O_3/ $ZnWO_4$ and $ZnWO_4$

The prominent diffraction peaks that the sample exhibited at 2θ = 15.46°,19°, 23.8°, 24.4°, 30.6°, 36.4°, 38.4°, 41.3°, 51.8° and 62° correspond to the (010), (100), (011), (110), (111), (021), (200), (121), (130), and (113) planes. These peaks can be indexed to the monoclinic wolframite structure of $ZnWO_4$, aligning well with the standard reference (JCPDS card no. 15-0774, space group $P_{2/c}$) [17]. This alignment confirms the absence of any other phases or impurities. Peaks at 29.5°, 34°, 36°, 44°, 48.8° and 58° are attributed to Er_2O_3 [18-19].

The morphology of $Er_2O_3/ZnWO_4$ is examined using SEM analysis in Fig.2. The $ZnWO_4$ appears to have a roughly spherical shape with a textured, granular surface. The surface morphology shows unevenly distributed smaller particles or clusters on the surface, which gives it a patterned appearance. This texture suggests possible agglomeration of Er_2O_3 particles on the surface of $ZnWO_4$, forming a larger composite structure.

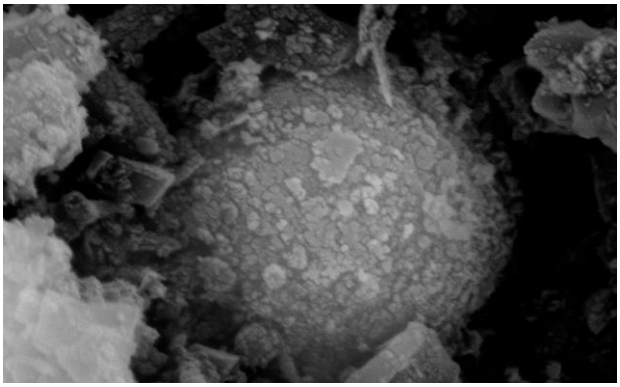

Fig. 2. SEM images of Er_2O_3/ $ZnWO_4$

3.2. Electrochemical performance of Er_2O_3/ $ZnWO_4$

The cyclic voltammetry (CV) graph in Fig.3. compares the electrochemical performance of $ZnWO_4$ and $Er_2O_3/ZnWO_4$ in a supercapacitor configuration, with current density (A g^{-1}) plotted against potential (V vs. Hg/HgO). The CV curves for $Er_2O_3/ZnWO_4$ exhibit more pronounced redox peaks compared to $ZnWO_4$, indicating stronger faradaic reactions, which are characteristic of pseudocapacitive behavior. This suggests that Er_2O_3 introduces additional redox-active sites, enhancing the charge storage capacity beyond what is provided by the electric double-layer capacitance. The $Er_2O_3/ZnWO_4$ composite also shows significantly higher current density than

$ZnWO_4$ alone across the potential range, implying an improvement in specific capacitance due to the synergistic effect of Er_2O_3. The area under the CV curve for $Er_2O_3/ZnWO_4$ is notably larger, suggesting increased charge storage and superior capacitive performance, making it more effective as an electrode material for supercapacitors. The potential window is approximately 0 to 0.6 V, typical for aqueous electrolytes like KOH, which offers stability in supercapacitor systems. The enhanced redox peaks in $Er_2O_3/ZnWO_4$ also suggest good reversibility and potential for high cyclic stability, important for long-term supercapacitor applications. The galvanostatic charge-discharge (GCD) curves for $ZnWO_4$ and $Er_2O_3/ZnWO_4$ electrodes shown in Fig.4. demonstrate notable differences in charge storage capacity, with potential plotted against time. Both curves show a linear charge-discharge profile, indicating stable capacitive behavior. However, the $Er_2O_3/ZnWO_4$ composite exhibits a significantly longer discharge time compared to $ZnWO_4$, suggesting an enhanced specific capacitance. This enhancement likely stems from the introduction of additional redox-active sites by Er_2O_3, which facilitates stronger faradaic reactions and thereby improves the overall charge storage. The linearity of the profiles also implies a balanced contribution from both double-layer capacitance and pseudocapacitance, with the $Er_2O_3/ZnWO_4$ composite benefiting from a greater pseudocapacitive effect. The Nyquist plot in Fig.5. illustrates the electrochemical impedance spectroscopy (EIS) data for $ZnWO_4$ and $Er_2O_3/ZnWO_4$ electrodes. In this plot, the x-axis represents the real component of impedance (Z') in ohms (Ω), while the y-axis displays the imaginary component (Z''). The graph highlights notable differences in impedance characteristics between the two materials. The semicircular section observed at high frequencies is associated with charge transfer resistance, and the subsequent linear segment at lower frequencies indicates diffusion-controlled behavior.

The smaller semicircle diameter for $Er_2O_3/ZnWO_4$ suggests it has a lower charge transfer resistance compared to the $ZnWO_4$. The larger arc observed for $Er_2O_3/ZnWO_4$ implies a higher overall impedance, which may result from enhanced faradaic reactions due to the addition of Er_2O_3. In the low-frequency region, both electrodes display a linear tail, which reflects their capacitive nature. The steeper slope for $Er_2O_3/ZnWO_4$ suggests improved ion diffusion and a more ideal capacitive performance. $Er_2O_3/ZnWO_4$ composite has better ion diffusion and pseudocapacitive characteristics, making it suitable for energy storage applications. The black line represents a fitted model, which aligns closely with the experimental data, indicating an accurate match for the impedance behavior of both materials.

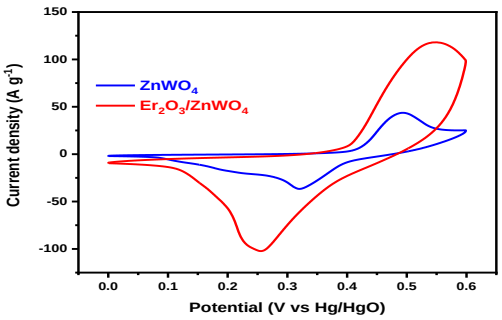

Fig.3. Cyclic voltammograms of $Er_2O_3/ZnWO_4$ and $ZnWO_4$.

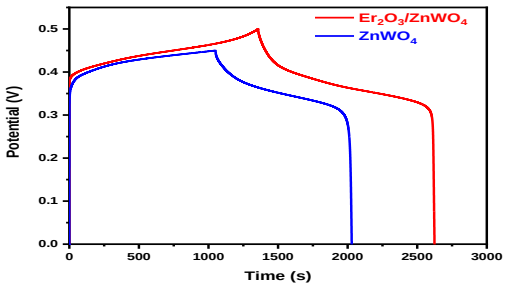

Fig.4. Galvanostatic charge-discharge of $Er_2O_3/ZnWO_4$ and $ZnWO_4$.

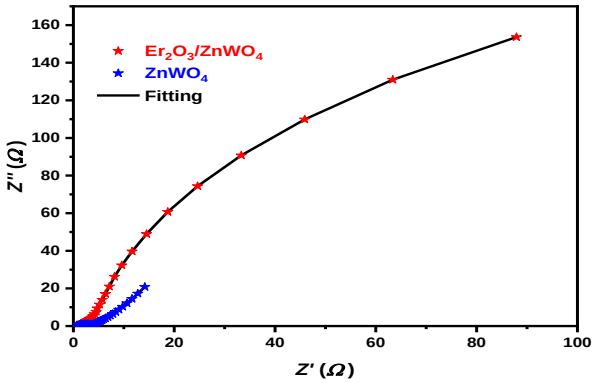

Fig.5. Nyquist plot for $Er_2O_3/ZnWO_4$ and $ZnWO_4$.

4. Conclusion

In summary, the electrochemical analysis of $ZnWO_4$ and $Er_2O_3/ZnWO_4$ composites reveals their promising applications in supercapacitors. The CV profiles show pseudocapacitive behavior for both materials, with $Er_2O_3/ZnWO_4$ exhibiting a higher current response, suggesting enhanced charge storage capabilities due to the addition of Er_2O_3. GCD measurements support these findings, with $Er_2O_3/ZnWO_4$ displaying a longer discharge period and greater specific capacitance, indicating improved energy retention.

Further insights are provided by the Nyquist plot, which highlights the impedance characteristics of each electrode. $Er_2O_3/ZnWO_4$ demonstrates lower charge transfer resistance, suggesting efficient electron movement and a larger semicircular arc, indicative of greater faradaic activity contributing to its enhanced capacitance. The steeper linear region in the low-frequency range for $Er_2O_3/ZnWO_4$ points to better ion diffusion, thereby improving its pseudocapacitive performance.

In conclusion, incorporating Er_2O_3 into $ZnWO_4$ significantly enhances the electrochemical properties, boosting specific capacitance, pseudo capacitance, and ion mobility. This enhancement makes the $Er_2O_3/ZnWO_4$ composite an excellent electrode material for supercapacitors, providing higher energy storage potential and superior stability compared to $ZnWO_4$ alone.

References

1. C.-J. Zhong, J. Luo, P.N. Njoki, D. Mott, B. Wanjala, R. Loukrakpam, S. Lim, L. Wang, B. Fang, Z. Xu, (2008) Fuel cell technology: nano-engineered multimetallic catalysts, Energy & Environmental Science, 1.
2. J. Yan, Q. Wang, T. Wei, Z. (2013) Fan, Recent Advances in Design and Fabrication of Electrochemical Supercapacitors with High Energy Densities, Advanced Energy Materials, 4.
3. R. Devanathan, (2008) Recent developments in proton exchange membranes for fuel cells, Energy & Environmental Science, 1.
4. J. Balamurugan, T.D. Thanh, N.H. Kim, J.H. Lee, (2016) Facile synthesis of 3D hierarchical N-doped graphene nanosheet/cobalt encapsulated carbon nanotubes for high energy density asymmetric supercapacitors, *Journal of Materials Chemistry A,* **4** 9555-9565.
5. G. Harichandran, P. Divya, J. Yesuraj, B. Muthuraaman, (2020) Sonochemical synthesis of chain-like $ZnWO_4$ nanoarchitectures for high performance supercapacitor electrode application, Materials Characterization, 167.
6. J. Zhang, X. Yang, Y. He, Y. Bai, L. Kang, H. Xu, F. Shi, Z. Lei, Z.-H. Liu, (2016) δ-MnO_2/holey graphene hybrid fiber for all-solid-state supercapacitor, *Journal of Materials Chemistry A*, **4** 9088-9096.
7. U. Nithiyanantham, S.R. Ede, T. Kesavan, P. Ragupathy, M.D. Mukadam, S.M. Yusuf, S. Kundu, (2014) Shape-selective formation of $MnWO_4$ nanomaterials on a DNA scaffold: magnetic, catalytic and supercapacitor studies, RSC Advances, **4**.
8. U. Nithiyanantham, S.R. Ede, S. Anantharaj, S. Kundu, (2014) Self-Assembled $NiWO_4$ Nanoparticles into Chain-like Aggregates on DNA Scaffold with Pronounced Catalytic and Supercapacitor Activities, Crystal Growth & Design, **15** 673-686.
9. S. Kundu, L. Ma, Y. Chen, H. Liang, (2017) Microwave assisted swift synthesis of $ZnWO_4$ nanomaterials: material for enhanced photo-catalytic activity, *Journal of Photochemistry and Photobiology A: Chemistry*, **346** 249-264.
10. Y. Wang, L. Liping, G. Li, (2017) Solvothermal synthesis, characterization and photocatalytic performance of Zn-rich $ZnWO_4$ nanocrystals, Applied Surface Science, **393** 159-167.
11. C. Li, Y. Liang, J. Mao, L. Ling, Z. Cui, X. Yang, S. Zhu, Z. Li, (2016) Enhancement of gas-sensing abilities in p-type $ZnWO_4$ by local modification of Pt nanoparticles, Anal Chim Acta, **927** 107-116.
12. Shobha, Bhaskaran, S.K. Gupta, (2021) High super capacitive performance of mixed transition and inner transition metal oxide-based hybrid nanostructures,

Materials Today: Proceedings, **43** 3221-3224.
13. P.D. Schumacher, J.L. Doyle, J.O. Schenk, S.B. Clark, (2013) Electroanalytical chemistry of lanthanides and actinides, Reviews in Analytical Chemistry, **32**.
14. M. Shoghi-Kalkhoran, F. Faridbod, P. Norouzi, M.R. Ganjali, (2017) Praseodymium molybdate nanoplates/reduced graphene oxide nanocomposite based electrode for simultaneous electrochemical determination of entacapone, levodopa and carbidopa, Journal of Materials Science: Materials in Electronics, **29** 20-31.
15. M. Rahimi-Nasrabadi, S.M. Pourmortazavi, M.S. Karimi, M. Aghazadeh, M.R. Ganjali, P. Norouzi, (2017) Erbium(III) tungstate nanoparticles; optimized synthesis and photocatalytic evaluation, *Journal of Materials Science: Materials in Electronics*, **28** 6399-6406.
16. U. Rajaji, S. Manavalan, S.M. Chen, S. Chinnapaiyan, T.W. Chen, R. Jothi (2019) Ramalingam, Facile synthesis and characterization of erbium oxide (Er_2O_3) nanospheres embellished on reduced graphene oxide nanomatrix for trace-level detection of a hazardous pollutant causing Methemoglobinaemia, Ultrason Sonochem, **56** 422-429.
17. B. Guan, L. Hu, G. Zhang, D. Guo, T. Fu, J. Li, H. Duan, C. Li, Q. Li, Facile (2014) synthesis of $ZnWO_4$ nanowall arrays on Ni foam for high performance supercapacitors, RSC Adv., **4** 4212-4217.
18. A. Bakhsh, A. Maqsood, (2012) Sintering effects on structure, morphology, and electrical properties of sol-gel synthesized, nano-crystalline erbium oxide, Electronic Materials Letters, **8** 605-608.
19. M. Elrouby, A.M. Abu-Dief, I.M. Mohamed, (2024) Facile synthesis and electrochemical characterization of erbium oxide and hydroxide for supercapacitor applications, Ionics, **30** 5699-5711.